JOURNAL OF THERMOPHYSICS AND HEAT TRANSFER
Vol. 21, No. 1, January–March 2007

Comparison of Heat Pumps for Permanent Lunar Base

M. A. Lambert*
San Diego State University, San Diego, California 92182-1323

DOI: 10.2514/1.21683

A permanent lunar habitat will require a heat pump to elevate waste heat from ∼298 K to ∼340–360 K to reject it from a reasonably sized radiator array because the effective sink temperature is 265 K for horizontal radiators at noon of the 336 h lunar daylight period. Because launch cost is proportional to mass, the figure of merit is overall mass of the external thermal control system: compressor, power source, radiators, heat exchangers, pumps, and piping. Previous investigations involved very detailed optimizations for electromechanical compressors. This investigation expands upon those by conducting a comprehensive assessment of thermally driven sorption heat pumps: absorption (liquid–vapor), adsorption (solid–vapor), and chemisorption (thermally reversible reaction between binder and refrigerant). The lowest mass alternative is a new design for an adsorption (carbon–methanol) heat pump with an overall system mass of 652 kg, as compared with 726 kg for an electromechanical compressor.

Nomenclature

A_{rad}	=	radiator emitting area, m^2
c_p	=	specific heat, $\text{J} \cdot \text{kg}^{-1} \cdot \text{K}^{-1}$
D_{coll}	=	outer diameter of collector tube in compound parabolic concentrator, m
h_{fg}	=	heat of vaporization, $\text{kJ} \cdot \text{kg}^{-1}$
k	=	thermal conductivity, $\text{W} \cdot \text{m}^{-1} \cdot \text{K}^{-1}$
L_{coll}	=	length of solar collector tube, m
$\dot{m}$	=	mass flow rate, $\text{kg} \cdot \text{s}^{-1}$
P	=	pressure, kPa or MPa
$\dot{Q}$	=	heat rate, W
q	=	heat flux, $\text{W} \cdot \text{m}^{-2}$
T_{lift}	=	temperature difference between evaporator and condenser, $T_{\text{lift}} = T_{\text{cond}} - T_{\text{evap}}$, K
ΔT	=	temperature difference, K
$\dot{W}_{\text{comp}}$	=	input energy (work) for electromechanical compressor, W
W_{ref}	=	width of parabolic solar reflector, m
α_S	=	solar absorptivity
ε_{IR}	=	infrared emissivity, 300 to 473 K
η_{Carnot}	=	Carnot thermodynamic efficiency
η_{fin}	=	fin efficiency
η_{focus}	=	focus quality (efficiency) of reflector for compound parabolic concentrator
θ	=	solar incidence angle measured from surface normal, deg
μ	=	dynamic viscosity, $\text{N} \cdot \text{s} \cdot \text{m}^{-2}$
ρ	=	density, $\text{kg} \cdot \text{m}^{-3}$
ρ_S	=	solar reflectivity

Subscripts

coll	=	solar collector tube
cond	=	condenser
EM	=	electromechanical
evap	=	evaporator
ref	=	parabolic reflector for concentrating solar thermal collector
SC	=	solar concentrator

Received 9 December 2005; revision received 28 March 2006; accepted for publication 29 March 2006.

*Assistant Professor, Department of Mechanical Engineering, MC 1323. Associate Fellow AIAA.

I. Introduction

NASA is redirecting its manned spaceflight program to extend beyond earth orbit, as part of its recently reinvigorated Space Exploration Initiative. The first step will be to establish a permanent lunar base (PLB) for researching the effects of reduced gravity and other aspects of living in space on human health and for serving as a starting point for manned exploration of Mars. A habitat is conceptualized in Fig. 1, providing living and working space for a crew of ∼6.

The most likely sites for a permanent lunar habitat are near the equator [1,2], where the lunar surface temperature soars to 384 K at noon of the lunar daylight period (14 Earth days) and plummets to 102 K during nighttime [3]. The moon's axis is inclined 1.53 deg to its orbital plane [2], and so at lunar noon near the equator the sun is almost directly overhead. These temperature extremes are why the six Apollo landings occurred at locations corresponding to early morning or late evening, where temperatures were closer to room temperature requiring less complex and bulky thermal control equipment during their brief stays (<2 Earth days). However, a permanent lunar base at midlatitudes would be subjected to these extremes of temperature.

The habitat has minimal heat exchange with the exterior because it is built with thick walls of insulating material to protect it from micrometeoroid impact [1]. Therefore, waste heat is entirely from interior sources. The most recent assessment of the cooling load is 15 kW for each of three independent cooling systems, which must be rejected by the external thermal control system (ETCS).† Human and plant metabolism, electronics, and machinery dissipate waste heat at ∼295–300 K (i.e., room temperature), which must be rejected to the exterior.

Waste heat is extracted by a chilled water circuit at $T_{\text{cool}} = 275$ K to avoid the possibility of a hazardous coolant contaminating the habitat in case of a leak [1]. The third most important consideration for the ETCS, after safety and reliability, is cost, which is largely dependent upon launch mass, now running about 10,000/kg to low Earth orbit (LEO) not to mention escape boosters and retrorockets for lunar landing.

The most practical and cost effective method for rejecting waste heat is to radiate it to space [1] rather than conducting it into the lunar regolith via very long cooling pipes buried a few meters beneath the surface, deeper than the layer heated by the daytime sun. (This is analogous to a "ground source/sink" terrestrial heat pump.)

At lunar noon at the equator, the sink temperature for vertical two-sided radiators is $T_{\text{sink}} = 324$ K with equal view factor (0.5) to both the hot lunar surface (384 K) and space (3 K). A specular parabolic radiator shade reduces heat exchange with the lunar surface [4,5],

†Private communication with Michael Ewert, Crew & Thermal Systems Division, NASA Johnson Space Center, November 2005.

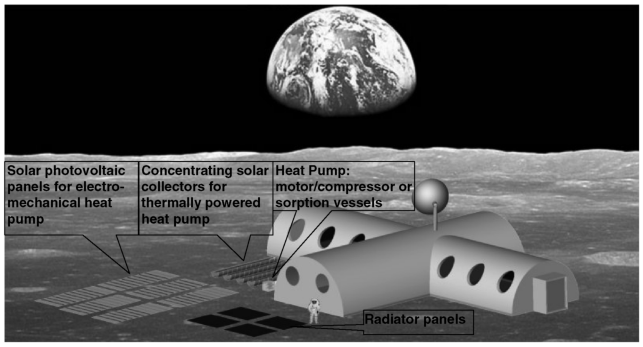

Fig. 1 Lunar habitat showing ETCS.

resulting in $T_{\text{sink}} = 195$ K. For a horizontal single-sided radiator $T_{\text{sink}} = 265$ K, the net effect of absorption of normally incident solar radiation ($G_S = 1371\ \text{W} \cdot \text{m}^{-2}$) and rejection to space. These sink temperatures are for radiators with end of life (EOL = 15 years), $\varepsilon_{\text{IR}} = 0.83$, and $\alpha_S = 0.17$ for a 250 μm thick silver Teflon coating [6]. The radiator array can comprise most of the ETCS mass [3].

To use unshaded vertical radiators, with $T_{\text{sink}} = 324\ \text{K} > T_{\text{cool}} = 275$ K, a heat pump is needed to elevate or "lift" the temperature of waste heat far enough above T_{sink} to permit using a reasonably sized radiator array. Horizontal radiators with $T_{\text{sink}} = 265$ K would have to be overly massive to reject heat at $T_{\text{rad}} = T_{\text{cool}} = 275$ K, because a minimum $\Delta T = T_{\text{rad}} - T_{\text{sink}} = 40$–$50$ K is needed to allow for a reasonably sized radiator array [1]. So, a heat pump is needed also for horizontal radiators. Shaded vertical radiators with $T_{\text{sink}} = 195$ K could use a simple pumped coolant loop without temperature "lift," but a heat pump would permit a smaller radiator array [4,5].

The mass of the heat pump and its attendant power system must be less than the reduction in radiator mass that they afford. So the most important design objectives are 1) maximize the efficiency, i.e., the coefficient of performance for cooling (COP_C), to minimize the mass of the photovoltaic array for electromechanical heat pumps or solar collectors for thermal heat pumps; 2) maximize the specific cooling power (SCP), $\text{W} \cdot \text{kg}^{-1}$, of the heat pump, or stated differently, minimize the mass penalty, $\text{kg} \cdot \text{kW}^{-1}$; and 3) ensure high reliability, requiring fewer redundant components.

II. Literature Review

A number of studies [1–3,7–12] of ETCS options for a lunar base were performed in the 1980s and 1990s. Eckert [13] summarized these in a comprehensive design protocol for a lunar base in 1999. Most ETCS studies concentrate on electromechanical vapor compression heat pumps powered by photovoltaic arrays, with $\text{COP}_C = 1.06$ to 1.50 and $\text{SCP} = 1000$ to $2000\ \text{W} \cdot \text{kg}^{-1}$. Some considered alternate power sources including gas turbines or thermoelectric generators powered by nuclear reactors or solar-thermal-electric generators taking the form of Stirling cycle engine generators mounted at the focus of paraboloidal "dish" concentrators.

One of the more recent studies, by Sridhar and Gottman [1], is a very detailed and comprehensive optimization of the design of the ETCS employing electromechanical heat pumps to reject a cooling load of $\dot{Q}_{\text{cool}} = 100$ kW. It uses state-of-the-art compressor performance available at that time and approximations for the mass penalty of nuclear powered generators ($30\ \text{kg} \cdot \text{kW}^{-1}$) and radiators ($2.5\ \text{kg} \cdot \text{m}^{-2}$) as deduced from several prior studies. Sridhar and Gottman [1] examined both reversed Rankine (vapor) and reversed Brayton (gas) devices, determining that R-11 (CCl_3F) and R-717 (NH_3) are the best refrigerants for the Rankine cycle whereas ethane is best for the Brayton cycle. The optimized Rankine cycle ETCS was only half as massive as the optimized Brayton cycle ETCS. For the Rankine cycle, Sridhar and Gottman [1] compared two architectures: 1) a single ETCS loop wherein the radiator is the condenser of the heat pump, and 2) a dual loop device with a heat pump loop and a radiator loop connected by a heat exchanger. For case 1, R-717 afforded lower ETCS mass (5515 kg at $T_{\text{rad}} = 362$ K) than R-11, even though R-11 yields higher efficiency in the heat pump, because R-717 is only a fraction of the density (~35%) of R-11 and has much better transport properties than R-11. For case 2, R-11 in the heat pump and R-717 in the radiator loop resulted in the lowest ETCS mass (5940 kg at $T_{\text{rad}} = 362$ K). Sridhar and Gottman [1] considered the optimized case 2, although 425 kg heavier (8%), to be superior because it offered better safety (e.g., from micrometeoroid damage) and operational control. They also considered reversed Stirling cycle heat pumps and noted that such devices were (and are) currently capable of providing only a few hundred watts of cooling, not the 15 kW necessary for a lunar base.

Hanford and Ewert [2] is another of the more recent studies which comprehensively assessed ETCS technologies for a permanent lunar base. That study also optimizes ETCS mass for electromechanical heat pumps using different assumptions than Sridhar and Gottman [1] for power mass penalty and radiators. Hanford and Ewert [2] used $20.2\ \text{kg} \cdot \text{kW}^{-1}$ for a dedicated solar photovoltaic array that was considered more feasible and much less expensive than a nuclear reactor. That investigation also considered current and proposed radiator designs settling upon mass penalties of $7.5\ \text{kg} \cdot \text{m}^{-2}$ for the horizontal and $5.0\ \text{kg} \cdot \text{m}^{-2}$ for the vertical, as derived from radiators employed on the International Space Station (ISS).

Hanford and Ewert [2] consider not only electromechanical heat pumps but also two thermally driven heat pumps: 1) zeolite and 2) complex compound. Zeolites are highly porous minerals that adsorb (i.e., reversibly bond with via van der Waals attraction) small polar refrigerants, particularly water, at low temperature and desorb them at high temperature [14]. Complex compound heat pumps [15] use chemisorption, a reversible thermally induced reaction between the refrigerant and a salt, e.g., NH_3 and $CaCl_2$.

For sorption devices, COP_C and SCP are inversely proportional because cycling them faster to increase SCP reduces their efficiency [16]. The zeolite heat pump considered by Hanford and Ewert [2] was inefficient with $\text{COP}_C = 0.40$, which required a massive radiator array and solar collector. Also, the low $\text{SCP} = 31.8\ \text{W} \cdot \text{kg}^{-1}$ meant the heat pump itself was quite massive. The complex compound heat pump considered by Hanford and Ewert [2] had even lower $\text{COP}_C = 0.30$, requiring an even more massive radiator array. But it had $\text{SCP} = 213\ \text{W} \cdot \text{kg}^{-1}$, making it only a fraction of the mass of the zeolite heat pump. Although sorption vessels are less efficient and more massive than electromechanical compressor/motors, solar collectors are only a fraction of the mass of photovoltaic arrays ($\sim 5\ \text{kg} \cdot \text{kW}^{-1}$ versus $>20\ \text{kg} \cdot \text{kW}^{-1}$), which is why Hanford and Ewert [2] also considered sorption devices.

Lynch [12] considered metal hydride heat pumps for planetary bases and spacecraft. These are chemisorption devices for which efficiency has recently been elevated to $\text{COP}_C = 0.90$ for a modest $T_{\text{lift}} = T_{\text{cond}} - T_{\text{evap}} \approx 40$ K, as reported by Klein and Groll [17]. Metal hydride heat pumps typically have $\text{SCP} = 30$–$50\ \text{W} \cdot \text{kg}^{-1}$ because a relatively small mass fraction of H_2 can be contained within the dense adsorbent (transition metals).

The most efficient adsorption heat pump prototype to date attained $\text{COP}_C = 1.2$ [18,19] for the zeolite–water pair. But its SCP was only $6.0\ \text{W} \cdot \text{kg}^{-1}$ because cooling power was sacrificed to achieve higher efficiency. The highest SCP achieved to date [20] is $220\ \text{W} \cdot \text{kg}^{-1}$ of the adsorbent, which translates to $\text{SCP} \approx 75$–$100\ \text{W} \cdot \text{kg}^{-1}$ of the heat pump (adsorbent plus containment vessel). Its efficiency was $\text{COP}_C = 0.80$ with the carbon–ammonia pair.

Lambert and Jones [21] describe an adsorption heat pump with innovations that increase predicted COP_C to 1.5 at $T_{\text{lift}} = 60$ K and predicted SCP to $355\ \text{W} \cdot \text{kg}^{-1}$ of the adsorbent and $141\ \text{W} \cdot \text{kg}^{-1}$ of the heat pump. The analytical model used to obtain the predicted enhancements was validated against the highest efficiency prototype to date [18,19].

The level of performance predicted or demonstrated for thermally powered heat pumps, as well as improvements in performance for small centrifugal compressors and motors, coupled with NASA's renewed intention to establish a PLB, warrants an updated assessment of the ETCS options.

III. External Thermal Control System Architectures

A. Internal Thermal Control System

1. Cooling Load

Before delving into the particulars of the ETCS, salient information on the internal thermal control system (ITCS) is described. Waste heat from internal sources is appreciable, mostly from equipment, and is currently estimated at 45 kW by NASA.[‡] It is assumed that solar tracking photovoltaic arrays will be used to provide constant power to internal equipment over the daylight period (14 Earth days).

Assuming a crew of at most 6, the total occupant heat rate would be only 0.87 kW, of which 0.45 kW is sensible and 0.42 kW is latent. This is deduced from an average occupant load of 145 W/person (=75 W sensible + 70 W latent) for an average daily activity level equivalent to seated light office work, more for higher activity and less for sleeping. The same result can be obtained by spreading daily caloric intake (3000 kcal) over 24 h. Showering, food warming, and transpiration from plants for experimentation or sustenance would add to the latent load, raising it to perhaps 1–2 kW, which is rather low compared with the total cooling load of 45 kW.

2. Internal Comfort Conditions

The interior of the habitat is cooled by chilled water [1,2] entering at $T_{\text{water}} = 275\ \text{K} = 2°\text{C}$. The chilled water acquisition loop rejects waste heat to the ETCS in a heat exchanger outside the habitat, which is the evaporator of the heat pump at $T_{\text{evap}} = 270\ \text{K}$. The interior is at about $T_{\text{dry bulb}} = 25°\text{C}$ (77°F), the midpoint of the summertime comfort band (23–26.5°C) at relatively low humidity, 35%, assuming lightweight clothing such as what shuttle astronauts wear. This has corresponding $T_{\text{dew}} = 8.5°\text{C}$. To remove the latent cooling load in a reasonably sized heat exchanger, the chilled water loop must be at least 5 K below $T_{\text{dew}} = 8.5°\text{C}$, which is the case because the water enters at $T_{\text{water}} = 2°\text{C}$.

B. Layout of the External Thermal Control System

The ETCS is composed of the following: 1) a compressor/motor for electromechanical heat pumps or sorption vessels and ancillary pumps and valves for thermally powered heat pumps; 2) solar photovoltaic (PV) panels for electromechanically driven systems or concentrating solar collectors for sorption devices (and a small PV array to power the heat transfer fluid pump); 3) a radiator, either a single-phase NH_3 heat exchanger (HEX) or a refrigerant condenser; 4) a HEX for connecting the ITCS chilled water circuit to the ETCS refrigerant circuit; 5) a second fluid–fluid HEX for electromechanical systems (not sorption) connecting the refrigerant circuit to the radiator circuit; and 6) a third fluid–fluid HEX for two-stage (cascaded) electromechanical systems connecting the low-temperature refrigerant loop to the high-temperature refrigerant loop.

C. Heat Pump Technologies

Although there are a number of types of devices for transferring heat from a cool source to a warm sink, only the following are feasible for rejecting the $\dot{Q}_{\text{cool}} = 15$ kW required of each of the three independent cooling systems for a lunar base: mechanical vapor compression, liquid–vapor absorption, solid–vapor adsorption, and chemisorption. Figures 2 and 3 depict schematics of four thermal control system (TCS) architectures representing the range considered.

1. Electromechanical Heat Pump

Figure 2 shows two electromechanical heat pumps. The left-hand side is the optimal configuration determined by Sridhar and Gottman [1], a single-stage (i.e., single-refrigerant loop) device with R-11 as the refrigerant, and a separate radiator loop (NH_3). The right-hand side is a two-stage ("cascade") variant employing 2 R-11 loops to achieve a given T_{lift} more efficiently, because COP_C decreases nonlinearly with T_{lift}, permitting a smaller photovoltaic array and a smaller radiator.

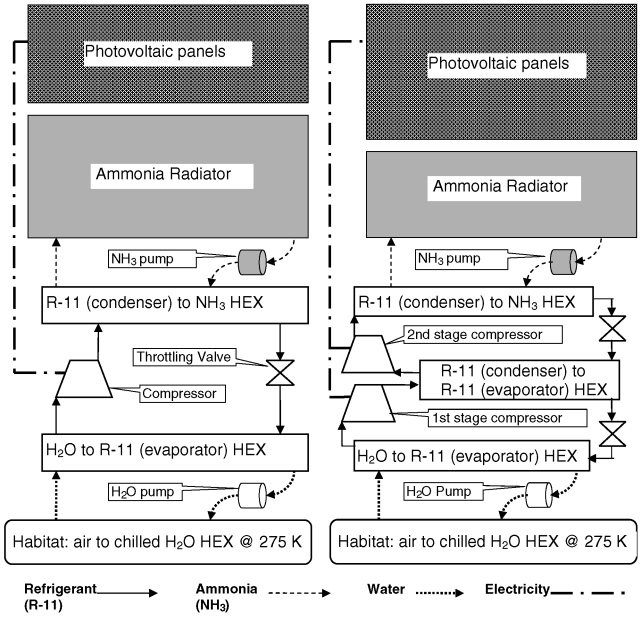

Fig. 2 Schematic diagrams of TCS employing electromechanical heat pumps.

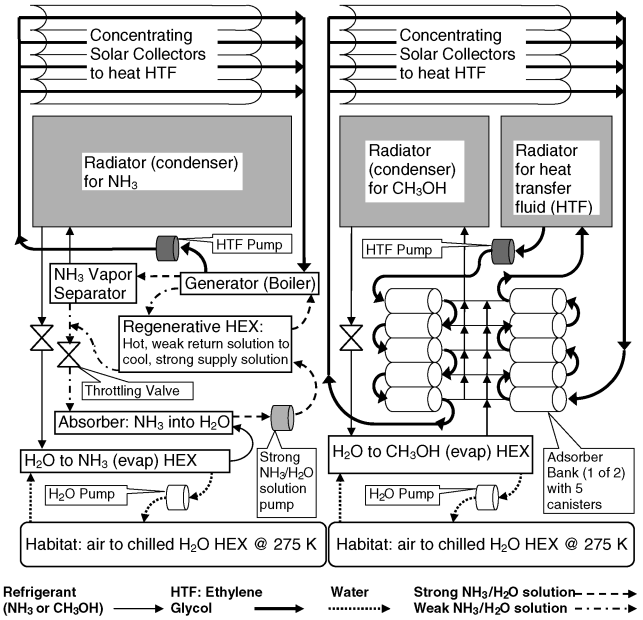

Fig. 3 Schematic diagrams of TCS employing thermal heat pumps. absorption (left), adsorption (right).

2. Absorption Heat Pump

Figure 3 shows an absorption heat pump (left-hand side). The compressor is the assemblage of an absorber vessel for dissolving either NH_3 into H_2O or H_2O into $LiBr/H_2O$ brine, a solution pump, a generator or boiler, a vapor separator to extract absorbent (solvent) from refrigerant, and a regenerative HEX for preheating the saturated solution going to the boiler with the depleted solution returning to the absorber.

The major difference between the absorption and mechanical compression systems is the primary form of energy used to drive the cycle. The mechanical compressor is replaced by a liquid pump, which requires only a fraction of the power (≈3–4%) to pump the

[‡]Private communication with Michael Ewert, Crew & Thermal Systems Division, NASA Johnson Space Center, November 2005.

much denser liquid working fluid to high pressure. A solar collector adds a large amount of heat to the generator to desorb refrigerant from absorbent. Absorption systems attain $COP_C \leq 0.70$ for "single-effect" heating cycles in which heat is used only once. Two-stage devices employ "double effect" heating (i.e., recycling of heat) to achieve $COP_C \leq 1.2$ but are bulkier, more complex, and costlier.

3. Adsorption Heat Pump

The compressor of the adsorption heat pump is the two banks of adsorbers shown in Fig. 3 (right-hand side). Solid–vapor adsorption operates on a principle similar to that of its better-known counterpart, liquid–vapor absorption. However, in solid–vapor heat pumps the refrigerant is adsorbed onto a solid desiccant (freeze dried) rather than absorbed into a liquid (dissolved) as in liquid–vapor heat pumps. Adsorption devices require a heat source at typically 150 to 250°C. Cyclically and asynchronously heating and cooling two or more adsorbers provides continuous cooling. Three adsorbent–refrigerant pairs have received attention: zeolite (a class of highly porous alumino-silicate minerals with cagelike crystalline lattices) and water; activated carbon and ammonia; and silica gel (highly porous SiO_2) and methanol.

Absorption and adsorption both are physical processes (physisorption), dissolution in the former and van der Waals (secondary) bonding in the latter. The strongest form of van der Waals bonding, hydrogen bonding, is exhibited by the small polar molecules H_2O, NH_3, and CH_3OH, which yield the best performance in adsorption heat pumps.

4. Chemisorption Heat Pump

Chemisorption heat pumps are those in which thermally reversible chemical reactions bind the refrigerant to the adsorbent. The "complex compound" heat pump employs an alkali or alkaline metal/halogen salt (e.g., NaCl) as the adsorbent and a small polar molecule (e.g., NH_3) as the refrigerant [15]. In the metal hydride heat pump, intermetallic compounds (of transition metals and/or rare earth metals) serve as the binder and hydrogen gas (H_2) as the refrigerant [12,17]. A chemisorption heat pump would have the same architecture as an adsorption heat pump and so is not depicted. Specifications for each of the architectures described here in Sec. III and illustrated in Figs. 2 and 3 are extracted from the literature and described in Sec. IV.

D. Reliability and Redundancy

Passive components, such as photovoltaic arrays, solar collectors, and radiators, can be plumbed or wired as multiple parallel units (with isolation valves at the inlets and outlets of collectors and radiators) to minimize the effect of failure of one or a few of them, such as from micrometeoroid damage. However, active components, such as compressors, pumps, and control valves, are by nature more prone to failure. For the purposes of this study, reliability of active components is addressed in the following discussion.

1. Electromechanical Heat Pump

For an electromechanical heat pump, failure of any of the many parts of either the compressor or its motor usually results in immediate loss of function. Because the entire cooling load is generated within the habitat, failure of the compressor/motor would require a near complete shut down of all equipment. If horizontal or shaded vertical radiators are employed, then a bypass liquid pump would be able to reject a small fraction of the nominal heat load. Redundancy of the compressor is therefore indispensable. So, it is assumed herein that each stage (whether one or two) has two compressor/motors in parallel, one as a spare or both used alternately. It is not uncommon for NASA designs to use tertiary redundancy of critical hardware. Similarly, it is assumed there are two parallel radiator coolant (ammonia) pumps.

2. Absorption Heat Pump

The solution pump is the principal active component requiring a spare, but its mass is only a small fraction of the total and is assumed to be subsumed into the total for the assemblage. The heat transfer fluid (HTF), ethylene glycol, circuit requires two parallel pumps.

3. Adsorption and Chemisorption Heat Pumps

The adsorbers are passive devices and are as reliable as other passive components such as radiators or photovoltaic panels. Each adsorber has two ball check valves, one to control flow of refrigerant from the adsorber to the condenser and another to control flow from the evaporator to the adsorber. Ball check valves are passive but do have moving parts (i.e., the spring and the ball bearing), yet these valves can last for millions of cycles. In the unlikely event that a ball check valve should fail, its associated adsorber would simply stop functioning. If there are 10 adsorbers, then the heat pump would still operate at 90% of full capacity. The mass of the adsorbers is increased by 10% to allow for an extra adsorber that can be connected to either bank.

As with absorption heat pumps, the HTF (ethylene glycol) circuit requires two parallel pumps. An active distribution manifold sequences HTF flow through the adsorbers, solar concentrators, and radiators. Being active, it requires a spare. The mass of each is ~5 kg.

IV. Performance of External Thermal Control System Components

A. Compressors

1. Mechanical Compressors, Electric Motors, and Liquid Pumps

Sridhar and Gottmann [1] determined that the reversed Rankine cycle affords the lowest ETCS mass for electromechanical heat pumps. Compressors are of four types: rotary vane, reciprocating, translating "scroll," and centrifugal, in order of least to greatest efficiency. The first three are positive displacement devices. State-of-the-art efficiencies, η_{Carnot}, and mass penalties, $\text{kg} \cdot \text{kW}^{-1}$, for compressors and motors from various sources [22–26] are listed in Table 1. Reciprocating and scroll compressor variants for automobiles have modest COP_C [22] and the highest SCP (lowest mass penalty) [23]. Scaringe [24] reported $\eta_{\text{Carnot}} = 80\%$ for a small centrifugal compressor (~20 kW) for use with halogenated refrigerants. This efficiency approaches that of medium-sized centrifugal compressors (in the 100s of kilowatt range).

The highest efficiency ac induction motors in the 10–15 kW range exhibit 90% efficiency [25], and dc motors of comparable power have 87% efficiency [26].

The overall efficiency of small output pumps (<0.5 kW fluid power) is about 40% [2].

Table 1 Highest efficiency mechanical compressors, pumps, and electric motors

Mechanical compressors, 10–15 kW cooling capacity	η_{Carnot}	Mass penalty, $\text{kg} \cdot \text{kW}^{-1}$	Electric motors, 5–15 kW, and controller	η_{Carnot}	Mass penalty, $\text{kg} \cdot \text{kW}^{-1}$
Reciprocating	0.61 [22]	0.52 [23]	ac induction [25]	0.90	1.0
Scroll	0.72 [22]	0.52 [23]	dc permanent magnet [26]	0.87	1.65
Centrifugal	0.80 [24]	0.45 [24]	dc power regulator [26]	0.983	2.3
Liquid pump	0.40 [2]	~2.5 [2]	For radiator fluid (NH_3) for electromechanical heat pumps or HTF (ethylene glycol) for sorption heat pumps.		

Table 2 Performance of thermally powered sorption compressors

Type of thermal heat pump	Working pair	Performance	η_{Carnot}	Mass penalty, $\text{kg} \cdot \text{kW}^{-1}$
Absorption	H_2O–NH_3	$\text{COP}_C = 1.2$ at $T_{\text{lift}} = 50$ K; $T_{\text{evap}} = 278$ K [27]	0.216	19 [28]
	$LiBr$–H_2O	$\text{COP}_C = 1.2$ at $T_{\text{lift}} = 50$ K; $T_{\text{evap}} = 278$ K [27]	0.216	19 [28]
Adsorption	Zeolite–H_2O	$\text{COP}_C = 0.4$ at $T_{\text{lift}} = 50$ K; $T_{\text{evap}} = 278$ K [2]	0.124	31
		$\text{COP}_C = 1.2$ at $T_{\text{lift}} = 50$ K; $T_{\text{evap}} = 278$ K [18,19]	0.216	83
	Carbon–NH_3	$\text{COP}_C = 0.8$ at $T_{\text{lift}} = 50$ K; $T_{\text{evap}} = 278$ K [20]	0.144	10
	SiO_2–CH_3OH	$\text{COP}_C = 0.8$ at $T_{\text{lift}} = 50$ K; $T_{\text{evap}} = 278$ K	0.144	10
	Carbon–CH_3OH	$\text{COP}_C = 1.6$ at $T_{\text{lift}} = 50$ K; $T_{\text{evap}} = 278$ K [21]	0.296	7.1
Chemisorption	$CaCl_2$–NH_3	$\text{COP}_C = 0.3$ at $T_{\text{lift}} = 50$ K; $T_{\text{evap}} = 278$ K [2]	0.083	4.7
		$\text{COP}_C = 1.0$ at $T_{\text{lift}} = 50$ K; $T_{\text{evap}} = 278$ K [15]	0.180	15.7
	Intermetallic–H_2	$\text{COP}_C = 0.9$ at $T_{\text{lift}} = 50$ K; $T_{\text{evap}} = 278$ K [17]	0.162	20

Table 3 Materials, properties, and sink temperatures for flow-through radiators

Radiator panel		Parabolic radiator shade	
Material: Graphite–epoxy face-sheets and ribs; aluminum alloy tubes [2]		***Material***: Aluminized Mylar®	
Coating: 0.25 mm silver Teflon		EOL, yr	5 (replaced twice)
EOL, yr	15	***Properties*** [6]: Specular top	$\varepsilon_{\text{IR}} = 0.06$
			$\alpha_S = 0.14$
Properties [6]:	$\varepsilon_{\text{IR}} = 0.83$	Diffuse bottom	$\varepsilon_{\text{IR}} = 0.90$
	$\alpha_S = 0.17$		$\alpha_S = 0.90$
	$\eta_{\text{fin}} = 0.85$		
		Area ratio: shade/radiator	2.30
Mass Penalty [2], $\mathbf{kg} \cdot \mathbf{m}^{-2}$		Mass penalty, $\text{kg} \cdot \text{m}^{-2}$	0.56
Horizontal	5.00	***Sink Temperature***: T_{sink}, K, at lunar noon	
Vertical	3.75	Horizontal	265
Shaded vertical [2,29]	7.61	Vertical	324
Working fluid; specific gravity = 1	0.63	Shaded vertical [29]	195

2. Thermally Powered Compressors

The performance of thermally powered compressors (absorption, adsorption, and chemisorption) is listed in Table 2. Double effect (two-stage) high capacity (>75 kW) absorption chillers can exhibit $\text{COP}_C = 1.2$ [27]. There is one maker of low capacity (e.g., residential) single-effect chillers [28] with $\text{COP}_C = 0.67$ and 18.4 kW cooling. Adding a second generator to raise COP_C to 1.2 (as for large capacity units) is estimated to result in a total mass penalty of 19 $\text{kg} \cdot \text{kW}^{-1}$.

The first zeolite–H_2O heat pump listed is the one modeled by Hanford and Ewert [2]. The second is that of Tchernev and Emerson [18] and Tchernev and Clinch [19], for which the actual mass penalty (167 $\text{kg} \cdot \text{kW}^{-1}$) has been halved by assuming the steel canister and copper internal heat exchanger are instead made of aluminum. Note that COP_C is increased by operating the unit at lower cooling capacity, thereby increasing mass penalty. The carbon–NH_3 heat pump [20] has the lowest experimental mass penalty to date (10 $\text{kg} \cdot \text{kW}^{-1}$). A silica gel–$CH_3OH$ device of the same configuration would yield similar performance. The last adsorption heat pump listed is that of Lambert and Jones [21], which is designed specifically for the lunar application to take advantage of the vacuum outside the habitat. This allows low operating pressure (280 kPa) and thin-walled adsorbers without the risk of atmospheric air leaking into the system and contaminating ("poisoning") the adsorbent or impeding two-phase heat transfer in the condenser (radiator) and evaporator.

The first chemisorption ($CaCl_2$–NH_3) heat pump listed is that modeled by Hanford and Ewert [2]. The second is a triple-effect (three stage) device which achieved much higher COP_C at the cost of much higher mass penalty [15]. The metal hydride heat pump developed by Klein and Groll [17] represents the state of the art for such devices.

B. Radiators

Hanford and Ewert [2] present a detailed review of radiators, those currently used on the International Space Station and on the space shuttle as well as proposed and prototype designs. Current radiators are all aluminum flow-through units using single-phase ammonia, because it has low ρ, μ, and T_{freeze} and high c_p and k. Hanford and Ewert [2] assess various advancements such as 1) flow-through radiators made largely of graphite fiber–epoxy composite instead of all aluminum, 2) composite thermosiphons that are passive (require gravity to operate), and 3) radiators with passive internal heat pipes.

Option 1 has been the favored option for the past decade.[§] Replacing the face sheets and the honeycomb between tubes of currently all aluminum radiators with graphite–epoxy composite reduces mass by 33.3% [2]. Properties and mass penalties of horizontal (one-sided), vertical (two-sided), and shaded vertical radiators are listed in Table 3. The mass penalty for a working fluid of specific gravity = 1 is 0.63 $\text{kg} \cdot \text{m}^{-2}$. This is adjusted for the actual specific gravity of the particular fluid for each type of heat pump (NH_3, CH_3OH, H_2O, H_2, or ethylene glycol). For the sorption devices, it is assumed the radiator tubing is 25% filled with liquid refrigerant because the condensation regime is annular flow for the low-mass flux in the radiator.

Sink temperatures, T_{sink}, for horizontal and vertical radiators are determined from Eqs. (1) and (2). The view factor from the vertical radiator to both the lunar surface and space is 0.5. Vertical radiators are aligned east–west so that the sun shines only on the top edge throughout daytime. The reflectivity (solar albedo) of a lunar mare or "sea" is only $\rho_{\text{moon}} = 0.07$, and so minimal sunlight is reflected onto vertical radiators. The net effect is a 1.3 K increase in T_{sink}. Horizontal:

$$T_{\text{sink}} = \left(\frac{\alpha_{S,\text{rad}} G_S \cos\theta}{\varepsilon_{\text{IR,rad}} \sigma} + T_{\text{space}}^4 \right)^{1/4} \tag{1}$$

Vertical:

$$T_{\text{sink}} = (0.5 T_{\text{moon}}^4 + 0.5 T_{\text{space}}^4)^{1/4} \tag{2}$$

Moon:

[§]Private communication with Michael Ewert, Crew & Thermal Systems Division, NASA Johnson Space Center, November 2005.

Table 4 T_{sink} throughout lunar day and night for horizontal and vertical radiators

θ, deg	Earth days from lunar noon	$\cos\theta$	T_{moon}, K	T_{sink} for horizontal radiator, K	T_{sink} for vertical radiator, K	T_{sink} for vertical radiator with parabolic specular shade, K
0	0	1	384	265	324	195
±10	0.8	0.985	383	264	323	194
±20	1.6	0.940	378	261	319	192
±30	2.3	0.866	371	256	313	188
±40	3.1	0.766	359	248	303	182
±50	3.9	0.643	344	238	290	175
±60	4.7	0.500	323	223	273	164
±70	5.4	0.342	294	203	248	149
±80	6.2	0.174	248	171	209	126
±90	7	0	173	3	145	86
Night	7	——	102	3	86	51

$$T_{moon} = \left(\frac{\alpha_{S,moon} G_S \cos\theta}{\varepsilon_{IR,moon}\sigma} + T_{space}^4 \right)^{1/4} \quad (3)$$

In order for computed T_{moon} to equal the measured 384 K at noon [3], $\alpha_S/\varepsilon_{IR}$ is set equal to 0.90. Lunar surface and sink temperatures are listed in Table 4.

Adding a parabolic specular reflective shade that is as tall as the radiator blocks all reflected sunlight (albedo) and infrared emission from the hot lunar surface (384 K). The focal line of the shade is just above the top edge of the radiator. The shade reduces T_{sink} to 195 K at lunar noon, as determined by Keller [29] using a numerical simulation, compared with 324 K without a shade. For a 1 m tall radiator, the parabolic arc length of the shade is 4.59 m, and the mass penalty for the shade and supports is 0.56 kg · m^{-2}. Because dust accumulation gradually changes reflectivity from specular to diffuse, thereby directing solar radiation onto the radiator, the shade is replaced at 5 year intervals, requiring three shades over the 15 year ETCS design lifetime [2].

The lightest radiator is a function of T_{rad} as shown in Fig. 4, a plot of mass penalty versus T_{rad}. Below $T_{rad} = 335$ K, shaded vertical radiators are lightest. For T_{rad} between 335 and 425 K, horizontal radiators are lightest, and above 425 K, vertical radiators are lightest.

Thermally powered heat pumps dissipate heat not only from the refrigerant (H_2O, NH_3, CH_3OH, or H_2) but also from the HTF (undiluted ethylene glycol). It is assumed PLB radiators would be similar in layout to those on the International Space Station. The pressure drop of ammonia through the parallel plumbed flow-through radiators of the ISS is $\Delta P_{ISS} = 372$ Pa · m^{-2} of radiator area. For ethylene glycol HTF

$$\Delta P_{HTF} = \Delta P_{ISS} \frac{(\rho c_p \Delta T_{out\text{-}in})_{NH_3}}{(\rho c_p \Delta T_{out\text{-}in})_{HTF}} \frac{\mu_{HTF}}{\mu_{NH_3}} = 2330 \text{ Pa} \cdot \text{m}^{-2} \quad (4)$$

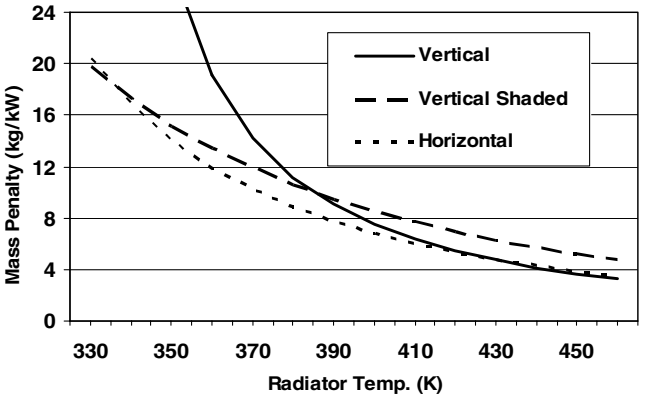

Fig. 4 Mass penalty versus radiator temperature.

C. Photovoltaic Generators

The photovoltaic panels for PLB internal systems track the sun to supply constant power throughout lunar daytime, resulting in constant cooling load. The power is inverted (dc/ac) and conditioned (regulated) as required by the electronics and appliances inside the habitat, adding substantial mass. The mass penalty [30] for inverted conditioned power is 35.3 kg · kW^{-1}.

Compressors and pumps for the ETCS can be run on either ac or dc power. Although the best ac motors are slightly more efficient than the best dc motors in the 5–15 kW range (see Table 1), noninverted minimally regulated dc power has a mass penalty of 20.2 kg · kW^{-1} for a nontracking horizontal array [30]. This is only 57% of the mass penalty for inverted conditioned ac power. Thus, the better choice for the ETCS is a dedicated noninverted (dc) nontracking array, at least at lunar noon.

However, output from horizontal nontracking arrays is proportional to the cosine of the solar incidence angle. T_{sink} also diminishes as θ increases, and so T_{lift} and $\dot{W}_{comp}$ can also be reduced while still rejecting the constant cooling load $\dot{Q}_{cool}$, meaning the compressor need not work as hard as at noon. But, available power may decrease too rapidly with increasing θ to permit enough lift to reject $\dot{Q}_{cool} + \dot{W}_{comp}$ from the radiator sized for noon.

Sridhar and Gottman [1] plotted COP_C versus T_{lift} for a centrifugal compressor (with R-11) modeled after lightweight aircraft air conditioning compressors, which are two-stage intercooled turbochargers driven by bleed air from the turbofans or auxiliary power unit:

$$\eta_{comp} = \eta_{mech}\eta_{elec}\eta_{control}\eta_{fluid} = 0.95 \times 0.94 \times 0.91 \times 0.75 = 0.609 \quad (5)$$

That plot is herein converted to a power law regression, Eq. (6), on the ideal efficiency $COP_{C,Carnot}$, which is plotted in Fig. 5. The average regression error is 1.3%:

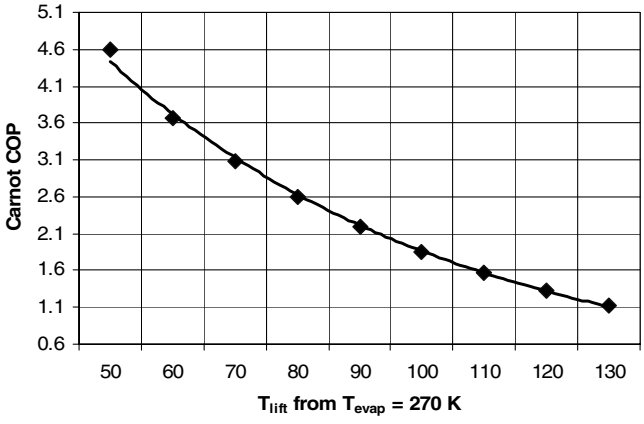

Fig. 5 $COP_{C,Carnot}$ versus T_{lift} for the centrifugal compressor modeled by Sridhar and Gottman [1].

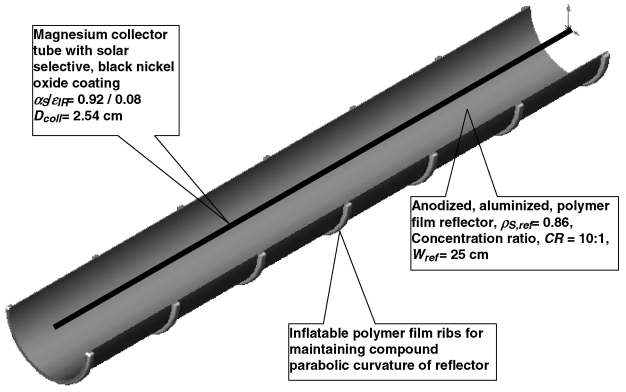

Fig. 6 Lightweight CPC solar collector to power sorption heat pumps.

$$\mathrm{COP}_{C,\mathrm{Carnot}} = 5.2669 \exp\lfloor -0.1732(0.1 \times (T_{\mathrm{lift}} + \Delta T_{\mathrm{cond}\to\mathrm{rad}}) - 4)\rfloor \tag{6}$$

This regression was reconverted to an actual COP_C based on the current state of the art in small (<20 kW) centrifugal compressors [24], dc motors [26], and controllers [26]:

$$\mathrm{COP}_C = \eta_{\mathrm{motor}}\eta_{\mathrm{control}}\eta_{\mathrm{fluid}}\mathrm{COP}_{C,\mathrm{Carnot}} = 0.684\mathrm{COP}_{C,\mathrm{Carnot}} \tag{7}$$

Although the higher η_{comp} used herein will alter optimal $T_{\mathrm{rad}} = 362$ K as computed by Sridhar and Gottman [1], $T_{\mathrm{rad}} = 362$ K is assumed to be a reasonable starting value for estimating the required radiator area as a function of θ. Adding $\Delta T_{\mathrm{cond}\to\mathrm{rad}} = 5$ K to $T_{\mathrm{rad}} = 362$ K yields $T_{\mathrm{cond}} = 367$ K. This is $T_{\mathrm{lift,noon}} = 97$ K above $T_{\mathrm{evap}} = 270$ K. Substituting $T_{\mathrm{lift}} = 97$ K into Eq. (6) and the resultant $\mathrm{COP}_{C,\mathrm{Carnot}}$ into Eq. (7) yields $\mathrm{COP}_C = 1.343$. The compressor work is

$$\dot{W}_{\mathrm{comp,noon}} = \dot{Q}_{\mathrm{cool}}/\mathrm{COP}_C = 11.2 \text{ kW} \tag{8}$$

Required radiator area at noontime is computed for a horizontal radiator, which is the best choice for 335 K < T_{rad} < 425 K (see Fig. 4):

$$A_{\mathrm{rad,noon}} = \frac{\dot{Q}_{\mathrm{cool}} + \dot{W}_{\mathrm{comp,noon}}}{\eta_{\mathrm{fin}}\varepsilon_{\mathrm{IR}}\sigma(T_{\mathrm{rad}}^4 - T_{\mathrm{sink}}^4)} = 53.5 \text{ m}^2 \tag{9}$$

Defining maximum (noontime) available power as $\dot{W}_{\mathrm{comp,noon}} = 11.2$ kW, which varies with $\cos\theta$, the required COP_C throughout the day is

$$\mathrm{COP}_C = \dot{Q}_{\mathrm{cool}}/(\dot{W}_{\mathrm{comp,noon}} \times \cos\theta) \tag{10}$$

Solving Eq. (6) for T_{lift},

$$T_{\mathrm{lift}} = 40 - \frac{10}{0.1732}\ell n\left(\frac{\mathrm{COP}_C}{0.684 \times 5.2669}\right) \tag{11}$$

$$A_{\mathrm{rad}} = \frac{\dot{Q}_{\mathrm{cool}} + \dot{W}_{\mathrm{comp,noon}} \times \cos\theta}{\eta_{\mathrm{fin}}\varepsilon_{\mathrm{IR}}\sigma[(T_{\mathrm{cool}} + T_{\mathrm{lift}} - \Delta T_{\mathrm{cond}\to\mathrm{rad}})^4 - T_{\mathrm{sink}}^4]} \tag{12}$$

Results of Eqs. (8–12) are listed in Table 5 over the course of the lunar day. The required A_{rad} increases with θ to approximately 105 m^2 at $T_{\mathrm{lift}} = 0$, below which the heat pump is unnecessary. Adding ~50 m^2 of horizontal radiators would add ~244 kg to the ETCS.

A better solution is to add tracking ability to the dedicated dc photovoltaic array. This would add 20–30% for frames, gimbals, gear-motors, and controllers, based on the percentage mass needed for support structures and deployment mechanisms for spacecraft radiators [2]. The average of 25% is assumed and added to the 20.2 kg · kW^{-1} for nontracking horizontal arrays, resulting in 25.3 kg · kW^{-1}. The added mass penalty for tracking dc photovoltaic arrays is 11.2 kW × (25.3 − 20.2) kg · kW^{-1} = 57 kg, only about 23% of the mass penalty of an additional 50 m^2 of horizontal radiators.

It is assumed that state-of-the-art triple-junction (InGaP/InGaAs/Ge) solar cells with the highest available conversion efficiency (27.5% beginning of life and 24.5% end of life) will be employed [31]. Although these are more efficient than silicon or germanium solar cells, they are also significantly thicker and heavier.

D. Solar Collectors

A compound parabolic concentrating (CPC) thermal collector is shown in Fig. 6. Its geometry, properties, and thermal performance are listed in Table 6 as sized for the carbon–methanol adsorption heat pump designed by Lambert and Jones [21]. The reflector is the same specular material used for the parabolic radiator shade and is also replaced at 5 year intervals over the 15 year design lifetime of the ETCS. The compound parabolic shape is maintained by inflatable ribs filled with low-pressure gas. The magnesium alloy collector tube is coated with solar-selective black nickel oxide ($\alpha_S/\varepsilon_{\mathrm{IR}}$ = 0.92/0.08) and is suspended by thin wires along the focal line of the CPC. The concentration ratio (CR) is 10:1 with a corresponding acceptance angle of ±5 deg, making it relatively easy to aim the axis at the sun during setup. The HTF is undiluted ethylene glycol with corrosion inhibitor additives (silicates, NaOH, and borate). The boiling point is 473 K at 1 bar (atm), which is equal to the selected outlet temperature meaning low pressure (<2 bar) can be used to prevent boiling.

The concentrating collector troughs are tracking, horizontal, and aligned north–south. The useful (captured) heat flux and efficiency are

Table 5 $\cos\theta$ compared with T_{lift} proportional to noontime T_{lift}

θ, deg	Earth days from lunar noon	$\cos\theta$	T_{sink} for horizontal radiator, K	COP_C	$\dot{W}_{\mathrm{comp}}$, kW	T_{lift}, K	A_{rad}, m^2
0	0	1	265	1.34	11.17	97.0	53.5
±10	0.8	0.985	264	1.36	11.00	96.1	53.6
±20	1.6	0.940	261	1.43	10.50	93.4	53.8
±30	2.3	0.866	256	1.55	9.68	88.7	54.3
±40	3.1	0.766	248	1.75	8.56	81.6	55.4
±50	3.9	0.643	238	2.09	7.18	71.5	57.5
±60	4.7	0.500	223	2.69	5.59	57.0	62.2
±70	5.4	0.342	203	3.93	3.82	35.1	73.4
±75	5.8	0.259	189	5.19	2.89	19.0	85.7
±80	6.2	0.174	171	7.73	1.94	−4.1	112.2
±90	7	0	3	15.41	0.97	−43.9	167.0
Night	7	——	3	——	——	——	——

Table 6 Geometry, properties, and performance of concentrating solar collector [21]

Parameter	Performance
Collector Tube: Magnesium alloy AZ31B	
Number of collector tubes, in parallel	10
D_{coll}, mm	25.4
L_{coll}, m	4.1
Metal mass per meter of tube, $\text{kg} \cdot \text{m}^{-1}$	0.218
$\alpha_{S,\text{coll}}$, EOL = 15 yr	0.92
$\varepsilon_{\text{IR,coll}}$ (EOL)	0.08
Metal + HTF mass penalty, $\text{kg} \cdot \text{m}^{-2}$	2.45
Solar tracking hardware, $\text{kg} \cdot \text{m}^{-2}$	0.50
Parabolic specular reflector	
Concentration ratio	10
A_{SC}, aperture area of collector, m^2	10.4
L_{ref}, m	4.1
W_{ref}, mm	254
$\alpha_{S,\text{ref}}$, EOL = 5 yr, replaced twice	0.14
$\rho_{S,\text{ref}}$ (EOL)	0.86
$\varepsilon_{\text{IR,ref}}$ (EOL)	0.06
η_{focus}	0.95
Reflector mass, $\text{kg} \cdot \text{m}^{-2}$	3×0.587
Heat transfer parameters	
G_S, solar irradiation, $\text{W} \cdot \text{m}^{-2}$	1371
T_{coll}, average collector tube temperature, K	462
q_{net}, net solar collection, $\text{W} \cdot \text{m}^{-2}$	966
η_{SC}, solar collector efficiency	0.704
$\dot{Q}_{\text{coll}}$ per meter of tube, $\text{W} \cdot \text{m}^{-1}$	245
Pressure drop ΔP_{SC}, Pa	**48**
Mass per unit area, $\text{kg} \cdot \text{m}^{-2}$	**4.71**
Power penalty, $\text{kg} \cdot \text{kW}^{-1}$	**4.88**

$$q_{\text{useful}} = \alpha_{S,\text{coll}}\rho_{S,\text{ref}}\eta_{\text{focus}}G_S - (\pi D_{\text{coll}}/W_{\text{ref}})\varepsilon_{\text{IR,coll}}\sigma(T_{\text{coll}}^4 - T_{\text{space}}^4) = 966\ \text{W} \cdot \text{m}^{-2} \tag{13}$$

$$\eta_{\text{SC}} = q_{\text{useful}}/G_S = 966/1371 = 0.704 \tag{14}$$

A prior design for a lightweight concentrating solar collector [7] (for water heating) is also inflatable but uses a cylindrical polymer film that completely encloses the collector tube, with the lower half aluminized or silvered and the upper half semitransparent. However, reflective losses are significant and increase with decreasing solar incidence angle. The open-top design [21] has minimal reflective losses.

E. Heat Exchangers

Figure 2 shows three HEX for the single-stage electromechanical heat pump and four HEX for the dual-stage architecture. The air-to-water heat exchanger inside the habitat is part of the ITCS and is common to all architectures, as is the external water-to-refrigerant heat exchanger, which is the first component in the ETCS. $\dot{Q}_{\text{cool}} = 15$ kW is assumed to include the pumping power for the heat acquisition chilled water loop. The mass penalty for two-phase or liquid heat exchangers [8] is $2.72\ \text{kg} \cdot \text{kW}^{-1}$.

The input energy, either work for electromechanical or heat for sorption, must be transferred in subsequent HEX, where $\dot{W}_{\text{comp}}$ (or $\dot{Q}_{\text{input}}$) $= \dot{Q}_{\text{cool}} \div \text{COP}_C$. This accounts for the "$1/\text{COP}_C$" in Eq. (15) for the mass of all ETCS HEX for a single-stage electromechanical heat pump:

$$m_{\text{HEX,EM,1-stage}} = 2.72 \times \dot{Q}_{\text{cool}}[1 + (1 + 1/\text{COP}_C)] \tag{15}$$

The dual-stage (cascade) electromechanical variant needs an additional (third) HEX in the ETCS to transfer heat from the second-stage R-11 circuit to the radiator circuit. The "2" exponent in Eq. (16) accounts for the additional $\dot{W}_{\text{comp}}$ added in the second-stage heat pump circuit:

$$m_{\text{Hex,EM,2-stage}} = 2.72 \times \dot{Q}_{\text{cool}}\lfloor 1 + (1 + 1/\text{COP}_C) + (1 + 1/\text{COP}_C)^2 \rfloor \tag{16}$$

The sorption heat pumps employ only one HEX in the ETCS, the water-to-refrigerant HEX that connects the ITCS to the ETCS. This is because H_2O, NH_3, and CH_3OH are considerably less dense and have much better transport properties than R-11. So there is no need to switch from a poor heat transport medium such as R-11 to NH_3 for the radiator. Therefore,

$$m_{\text{HEX,thermal}} = 2.72 \times \dot{Q}_{\text{cool}}[1] \tag{17}$$

F. Piping and Cabling

It is assumed that the radiators, solar concentrators, dedicated PV array, and compressors (electromechanical or sorption) are 25 m from the ITCS–ETCS junction (chilled water-to-refrigerant HEX) on the outside of the habitat to lessen dust accumulation on these components. Therefore 50 m of refrigerant piping are needed for the supply and return lines (25 m each) from the compressor to the radiator array. The supply line is full of liquid and the return line is full of vapor of negligible mass. For thermally driven heat pumps, 25 m of ethylene glycol filled piping is needed to connect the solar concentrators and radiators to the sorption compressors. The piping is magnesium alloy, internally anodized, with OD = 19.1 mm and ID = 17.3 mm. This is large enough to ensure that ΔP is small enough to not affect performance of the radiator.

The mechanical compressor and pump motors are assumed to operate on 96 V dc, the typical limit for commercially available items. The allowable voltage drop is set to 1% ($\sim$1 V dc) because the power mass penalty is substantial ($25.3\ \text{kg} \cdot \text{kW}^{-1}$), and so the supply voltage is 97 V dc. Twenty-five meters of insulated aluminum cabling is needed to connect the PV array to the compressors. Piping and cabling account for $\sim$2% of the ETCS mass.

V. Comparison of Heat Pump Technologies for External Thermal Control Systems

A. Principal Figure of Merit: Overall Mass of External Thermal Control Systems

The main objective is to identify the ETCS architecture with the lowest mass, including any redundancy necessary to ensure reliability, and features that minimize any possible risks (e.g., using chilled water instead of other refrigerants for the ITCS). Mass is very important because launch cost is proportional to mass and is currently greater than $10,000/\text{kg}$ to reach LEO, not to mention transport to and landing on the moon.

B. Evaluation of Compressor Options

Criteria for computing masses of the components of the heat pumps shown in Figs. 2 and 3 are described in detail in Sec. IV. Table 7 lists performance criteria (COP_C, η_{Carnot}, T_{lift}, and T_{rad}) and masses of all ETCS components for optimized variants of the four types of heat pumps considered: mechanical, absorption, adsorption, and chemisorption. Optimization was achieved by varying T_{lift} to obtain the lowest overall ETCS mass. Table 7 is divided into two main sections, mechanical compression and thermal compression systems, and the latter is further differentiated into physical sorption (absorption and adsorption) and chemical sorption.

1. Electromechanical

The lightest option is a single-stage device with a centrifugal compressor requiring a total ETCS mass of 726 kg at $T_{\text{lift}} = 78$ K with corresponding $T_{\text{rad}} = 343$ K. The small capacity (5–10 kW flow work) centrifugal compressor is something of a novelty because it is very expensive and worth considering only when efficiency is paramount, as for a PLB. But its long-term (15 year) reliability must be verified. Therefore, results are included for less efficient reciprocating and scroll compressors, because these have been

Table 7 Mass breakdown of various ETCS architectures for a permanent lunar base

		η_{Carnot}	COP_C per stage	COP_C total	T_{lift} per stage, K	T_{lift} net, K	T_{rad}, K	T_{sink}, K	Compressor	Solar PV array	Solar CPC	Radiator	HEX	Pumps	Piping and cabling	Total ETCS mass, kg
Mechanical compression																
Reciprocating:	two-stage	0.522	2.52	1.05	45	80	350	265	89	371	——	391	177	2.0	24	1055
	one-stage	0.522	1.52	1.52	74	69	339	265	50	257	——	404	108	1.8	20	842
Scroll:	two-stage	0.616	2.87	1.22	47	84	354	265	82	319	——	340	170	1.7	22	934
	one-stage	0.616	1.74	1.74	76	71	341	265	46	226	——	370	105	1.6	19	768
Centrifugal:	two-stage	0.684	3.08	1.33	49	88	358	265	78	294	——	307	166	1.5	21	868
	one-stage	0.684	1.87	1.87	78	73	343	265	44	210	——	348	103	1.5	18	726
Thermal compression																
Absorption:	H_2O–NH_3	0.216	0.62	0.62	84	84	354	265	284	19	119	474	41	4.0	17	958
	LiBr–H_2O	0.216	0.62	0.62	84	84	354	265	284	19	119	481	41	4.0	20	967
Adsorption:	Zeolite–H_2O	0.216	0.62	0.62	84	84	354	265	1250	19	119	481	41	4.0	20	1933
	Carbon–NH_3	0.144	0.47	0.47	77	77	347	265	150	22	156	637	41	4.5	17	1028
	Silica gel–CH_3OH	0.144	0.47	0.47	77	77	347	265	150	22	156	642	41	4.5	18	1034
	Carbon–CH_3OH	0.333	0.77	0.77	95	95	365	265	127	18	93	352	41	3.8	18	652
Chemisorption:	$CaCl_2$–NH_3	0.180	0.54	0.54	81	81	351	265	235	20	135	539	41	4.2	17	991
	Metal hydride–H_2	0.162	0.51	0.51	79	79	349	265	300	21	144	574	41	4.3	13	1098

proven to perform for 20 years or more. Although no active component can be considered so reliable that redundancy can be foregone, unless redundancy is impossible (e.g., the ascent engine for the Apollo program lunar module). The ETCS mass with a scroll compressor is 768 kg at $T_{lift} = 76$ K and $T_{rad} = 341$ K.

Dual-stage or cascade cycles are also considered because nominally halving the large T_{lift} for a single-stage device affords higher COP_C. The two stages must "overlap" (Fig. 2, right-hand side), that is, T_{cond} of the lower temperature loop must be higher than T_{evap} of the higher temperature loop by at least $\Delta T = 5$ K to allow for a reasonably sized interloop heat exchanger [1]. But the extra mass of the interloop HEX, higher required capacity and therefore mass of the second-stage compressor, and reduction of efficiency due to temperature overlap in the interloop HEX between the first and second stages requires a greater overall ETCS mass.

2. *Absorption*

Absorption heat pumps require ETCS masses of 958 kg for NH_3–H_2O and 967 kg for LiBr–H_2O, both at $T_{lift} = 84$ K and $T_{rad} = 354$ K. The hardware mass of the absorption system (absorber, vapor generator, vapor separator, and internal regenerative heat exchanger) is much greater than an electromechanical compressor of equal capacity. The lower COP_C requires a more massive radiator. But the solar collector for the absorption heat pump is much lighter than the PV array for the mechanical device.

3. *Adsorption*

The lightest ETCS using a sorption device based on experimental performance of the state-of-the-art bench-scale prototype [20] is the activated carbon–NH_3 variant with total ETCS mass of 1028 kg at $T_{lift} = 77$ K and $T_{rad} = 347$ K.

The activated carbon–CH_3OH heat pump with overall ETCS mass of 652 kg at $T_{lift} = 95$ K and $T_{rad} = 365$ K is based on a new design [21]. The analytical model used to predict its performance has been validated against the highest COP_C prototype tested and reported in the literature [18,19].

4. *Chemisorption*

The complex compound ($CaCl_2$–NH_3) heat pump has an overall ETCS mass of 991 kg at $T_{lift} = 81$ K and $T_{rad} = 351$ K.

VI. Conclusions

The present work builds upon comprehensive detailed studies [1–3,7–12] of heat pump options for the ETCS of a PLB. These earlier works focused mainly upon electromechanical heat pumps. This investigation provides the most inclusive and detailed assessment of thermally driven sorption heat pumps. The impetus for this comparison is the design of a new adsorption (carbon–methanol) heat pump with increased efficiency (COP_C) and SCP (kW cooling/kg of heat pump). The following conclusions are obtained from this investigation:

1) The lightest option is an adsorption (carbon–methanol) heat pump with overall ETCS mass of 652 kg, as compared with 726 kg for the lightest electromechanical heat pump with a centrifugal compressor. The overall mass savings afforded by the sorption device for three identical ETCS is 222 kg, which correlates to a launch cost savings of \$2.2 million at a conservative 10,000/kg to LEO. This would be multiplied by a factor of 2 to 3 to include the cost of the orbital escape booster and lunar landing retrorocket.

2) The adsorption heat pump is modular with 10 sorption vessels that are "solid state" with no moving parts except a pair of passive check valves. The HTF pump and distribution manifold are the only active components that are at least as reliable as mechanical compressors.

3) Vertical radiators with specular parabolic shades afford the lowest mass penalty ($kg \cdot kW^{-1}$) for radiator temperature up to $T_{rad} = 335$ K. For $335 < T_{rad} < 425$ K, horizontal radiators have the lowest mass penalty. And above 425 K, unshaded vertical radiators

are best. Horizontal radiators are the best choice for all heat pump technologies considered herein, mechanical compression and sorption, with T_{rad} between 339 and 365 K.

4) A dedicated nontracking noninverted (dc) minimally regulated PV array has the lowest mass penalty (20.2 kg · kW^{-1}). But if the PV array and radiator are exactly sized for noontime conditions, then the PV array cannot provide enough power to reject all waste heat during lunar "morning" and "evening." Thus, the dedicated PV array must have tracking ability, which is estimated to add 25% to its mass penalty.

Acknowledgement

The author would like to thank Michael K. Ewert at the Crew & Thermal Systems Division, NASA Johnson Space Center, for data and insights on heat pumps for space applications.

References

[1] Sridhar, K. R., and Gottmann, M., "Thermal Control System for Lunar Base Cooling," *Journal of Thermophysics and Heat Transfer*, Vol. 10, No. 3, July–Sep. 1996, pp. 490–496.

[2] Hanford, A. J., and Ewert, M. K., "Advanced Active Thermal Control Systems Architecture Study," NASA TM-104822, Oct. 1996.

[3] Ewert, M. K., Petete, P. A., and Dzenitis, J., "Active Thermal Control Systems for Lunar and Martian Exploration," *Advanced Environmental/Thermal Control and Life Support Systems: 20th Intersociety Conference on Environmental Systems*, SP-831, Society of Automotive Engineers, Warrendale, PA, 1990; also Society of Automotive Engineers Paper 90-1243, July 1990.

[4] Costello, F. A., and Swanson, T. D., "Lunar Radiators with Specular Reflectors," *Heat Transfer in Space Systems*, edited by S. H. Chan, E. E. Anderson, R. J. Simoneau, C. H. Chan, D. W. Pepper, and B. F. Blackwell, American Society of Mechanical Engineers, New York, 1990, pp. 145–150.

[5] Ewert, M. K., Graf, J. P., and Keller, J. P., "Development of Lunar Radiator Parabolic Shading System," *25th Intersociety Conference on Environmental Systems*, Society of Automotive Engineers Paper 95-1524, 1995.

[6] Peck, S., "Radiator Panel Coating Comparisons," Long Duration Exposure Facility (LDEF) Test Results, LTV Corp., report, Cleveland, OH, Aug. 1990.

[7] Simonsen, L. C., DeBarro, M. J., Farmer, J. T., and Thomas, C. C., "Conceptual Design of a Lunar Base Thermal Control System," *Symposium on Lunar Base and Space Activities in the 21st Century*, Lunar Base & Space Paper 88-225, April 1988.

[8] Swanson, T. D., Radermacher, R., Costello, F. A., Moore, J. S., and Mengers, D. R., "Low Temperature Thermal Control for a Lunar Base," *Advanced Environmental/Thermal Control and Life Support Systems: 20th Intersociety Conference on Environmental Systems*, SP-831, Society of Automotive Engineers, Warrendale, PA, 1990; also Society of Automotive Engineers Paper 90-1242, July 1990.

[9] Ewert, M. K., "Investigation of Lunar Base Thermal Control System Options," *23rd International Conference on Environmental Systems*, Society of Automotive Engineers Paper 93-2112, July 1993.

[10] Swanson, T. D., Sridhar, K. R., and Gottmann, M., "Moderate Temperature Control Technology for a Lunar Base," *23rd International Conference on Environmental Systems*, Society of Automotive Engineers Paper 93–2114, July 1993.

[11] Ewert, M. K., Keller, J. R., and Hughes, B., "Conceptual Design of a Solar Powered Heat Pump for Lunar Base Thermal Control System," *26th International Conference on Environmental Systems*, SAE Paper 96-1535, July 1996.

[12] Lynch, F. E., "Metal Hydride Thermal Management Techniques for Future Spacecraft and Planetary Bases, Phase 1: Final Report," Hydrogen Consultants, Inc., Document ID: 19930072568, Aug. 1987; also NASA CR-190993, Center for Aerospace Information, Aug. 1987.

[13] Eckert, P., "Thermal Control Systems," *The Lunar Base Handbook*, McGraw–Hill, New York, 1999, Chap. 11.

[14] Tchernev, D. I., "Natural Zeolites in Solar Energy Heating, Cooling, and Energy Storage," *Reviews in Mineralogy and Geochemistry*, , edited by D. L. Bish and D. W. Ming, Vol. 45, Natural Zeolites: Occurrence, Properties, Applications, Mineralogical Society of America, Chantilly, VA, 2000, Chap. 17, pp. 589–617.

[15] Rockenfeller, U., Kirol, L., and Khalili, K., "High Temperature Waste-Heat Driven Cooling Using Complex Compound Sorption Media, Phase 2: SBIR Final Report," Rocky Research, Boulder City, NV, Jan. 1996.

[16] Lambert, M. A., and Jones, B. J., "Review of Regenerative Adsorption Heat Pumps," *Journal of Thermophysics and Heat Transfer*, Vol. 19, No. 4, Oct.–Dec. 2005, pp. 471–485; also AIAA Paper 2003-0514.

[17] Klein, H. P., and Groll, M., "Development of a Two-Stage Metal Hydride System as Topping Cycle in Cascading Sorption Systems for Cold Generation," *Applied Thermal Engineering*, Vol. 22, No. 6, 2002, pp. 631–639.

[18] Tchernev, D. I., and Emerson, D. T., "High-Efficiency Regenerative Zeolite Heat Pump," *ASHRAE Transactions*, Vol. 94, No. 3, 1988, pp. 2024–2032.

[19] Tchernev, D. I., and Clinch, J. M., "Closed Cycle Zeolite Regenerative Heat Pump," *Proceedings of the ASME 11th Annual Solar Energy Conference*, American Society of Mechanical Engineers, New York, 1989, pp. 347–351.

[20] Miles, D. J., Sanborn, D. M., Nowakowski, G. A., and Shelton, S. V., "Gas-Fired Sorption Heat Pump Development," *Heat Recovery Systems and Combined Heat and Power*, Vol. 13, No. 4, 1993, pp. 347–351.

[21] Lambert, M. A., and Jones, B. J., "A Solar Powered Adsorption Heat Pump," U.S. Patent Application, Docket No. BSDSU 1033526, filed 23 Nov. 2005; also Lambert, M. A., and Jones, B. J., "Design of Adsorption Heat Pump for Permanent Lunar Base," *Journal of Thermophysics and Heat Transfer*, Vol. XX, No. XX, 2006, pp. XXX–XXX.

[22] Christy, C., Fusco, D., and Toossi, R., "Adsorption Air Conditioning for Containerships and Vehicle, Final Report," METRANS Center Contract No. 65A0047, California State University–Long Beach, Long Beach, CA, 27 June 2001.

[23] Bhatti, M. S., "Evolution of Automotive Air Conditioning, Riding in Comfort, Part 2," *ASHRAE Journal*, Vol. 41, No. 9, Sept. 1999, pp. 44–50.

[24] Scaringe, R. P., presentation at NASA Johnson Space Center, Mainstream Engineering Corp., Rockledge, FL, July 1997.

[25] Appelt, D., "Thermal Control of an AC Induction Motor for a Hybrid Electric Vehicle," M.S. Thesis, Dept. of Mechanical Engineering, San Diego State Univ., San Diego, CA, Aug. 2004.

[26] PENTAD G, permanent magnet double vented dc motor, PENTAD, Thousand Oaks, CA, product webpage http://home.earthlink.net/~glraymond/pentadpg.html [cited 20 March 2006].

[27] Parsons, R. A. (ed.), *2000 ASHRAE Handbook: Air Conditioning Systems and Equipment*, American Society of Heating, Refrigerating, and Air Conditioning Engineers, Atlanta, GA, 2000.

[28] Robur GAHP-W, water-cooled gas absorption heat pump, 18.4 kW cooling capacity, Robur, Zingonia, Italy, product webpage http://www.robur.com/pag_prodotto.jsp?idp=18&idl=2&steps=0 [cited 26 March 2006].

[29] Keller, J. R., "Full and Partial Parabolic Shade Modeling Using the Thermal Synthesizer System (TSS)," NASA Report CTSD-1829, 1994; also Lockheed Engineering and Sciences Company Report LESC-31341, Houston, TX, 1994.

[30] Hughes, M. B., "Lunar Base Power System for Solar Heat Pumps," NASA Report HDID-E-96-191, 1995; also Lockheed Martin Engineering and Sciences Company Report LMES-31919, Houston, TX, 1995.

[31] Advanced triple-junction (ATJ: n/p InGaP/InGaAs/Ge) solar photovoltaic cells for space applications, Emcore Photvoltaics, Albuquerque, NM, product webpage http://www.emcore.com/product/photovoltaic.php [cited 14 Oct. 2006].